

Article

Charged Particles Orbiting Charged Black-Bounce Black Holes

Sardor Murodov ^{1,2,3} , Kodir Badalov ^{1,2,3} , Javlon Rayimbaev ^{4,5,6,7,*} , Bobomurat Ahmedov ^{1,8,9} 
and Zdeněk Stuchlík ¹⁰

- ¹ Institute of Fundamental and Applied Research, National Research University TIIAME, Kori Niyoziy 39, Tashkent 100000, Uzbekistan; mursardor@ifar.uz (S.M.); b-qodir@samdu.uz (K.B.); ahmedov@astrin.uz (B.A.)
² Uzbek—Finnish Pedagogical Institute, Spitamen Shokh Str. 166, Samarkand 140100, Uzbekistan
³ Department of Theoretical Physics, Samarkand State University, Samarkand 140104, Uzbekistan
⁴ School of Mathematics and Natural Sciences, New Uzbekistan University, Movarounnahr Str. 1, Tashkent 100007, Uzbekistan
⁵ School of Engineering, Central Asian University, Tashkent 111221, Uzbekistan
⁶ Faculty of Computer Engineering, University of Tashkent for Applied Sciences, Gavhar Str. 1, Tashkent 100149, Uzbekistan
⁷ Power Engineering Faculty, Tashkent State Technical University, Tashkent 100095, Uzbekistan
⁸ Institute of Theoretical Physics, National University of Uzbekistan, Tashkent 100174, Uzbekistan
⁹ Ulugh Beg Astronomical Institute, Astronomy St. 33, Tashkent 100052, Uzbekistan
¹⁰ Research Centre for Theoretical Physics and Astrophysics, Institute of Physics, Silesian University in Opava, Bezručovo nám. 13, CZ-74601 Opava, Czech Republic; zdenek.stuchlik@physics.slu.cz
* Correspondence: javlon@astrin.uz

Abstract: The detailed and comprehensive analysis of radiation processes in accretion disks consisting of electrically charged particles around black holes may provide powerful information about the spacetime geometry of the central black hole. We investigate the circular orbits of electrically charged particles around an electrically charged black-bounce Reissner–Nordström (RN) black hole, known as an RN Simpson–Visser (SV) black hole. We also study the profiles of the innermost stable circular orbits (ISCOs), energy, and angular momentum of the particles in their ISCOs, as well as the efficiency of energy release processes in the accretion disk in the Novikov–Thorne model. Finally, we calculate and study the effects of the black-bounce parameter as well as the black-hole charge on the intensity of the radiation of ultrarelativistic charged particles orbiting the charged RN SV black hole along circular orbits and falling into the black hole. It is observed that the black-bounce parameter essentially decreases the ISCO radius, and consequently the energy extraction and intensity of electromagnetic radiation.

Keywords: black-bounce black hole; Simpson–Visser spacetime; ISCO; charged particles; radiation intensity



Citation: Murodov, S.; Badalov, K.; Rayimbaev, J.; Ahmedov, B.; Stuchlík, Z. Charged Particles Orbiting Charged Black-Bounce Black Holes. *Symmetry* **2024**, *16*, 109. <https://doi.org/10.3390/sym16010109>

Academic Editor: Jose Antonio de Freitas Pacheco

Received: 27 December 2023

Revised: 11 January 2024

Accepted: 15 January 2024

Published: 16 January 2024



Copyright: © 2024 by the authors. Licensee MDPI, Basel, Switzerland. This article is an open access article distributed under the terms and conditions of the Creative Commons Attribution (CC BY) license (<https://creativecommons.org/licenses/by/4.0/>).

1. Introduction

Black holes are often described in astrophysical scenarios as rotating compact objects characterized by their spin parameter, which is responsible for their energetics. The first exact solutions for charged black holes were derived independently by Reissner and Nordström and involved a combination of general relativity (GR) and linear Maxwell electrodynamics [1,2]. These solutions, known as RN black holes, introduced the concept of electric charge for black holes but suffered from a physical singularity.

To address the singularity problem, researchers have explored exact solutions for charged black holes in GR combined with nonlinear electrodynamics. These solutions, termed regular (rotating)-black-hole solutions, were proposed by scientists in the literature [3–8]. These regular-black-hole solutions aim to provide alternatives that avoid or mitigate the issues associated with physical singularities, often by introducing nonlinearity modifications to the standard Maxwell equations.

For the first time, Simpson and Visser introduced a straightforward method to address singularity issues by modifying the metric through the coordinate transformation r with $\sqrt{r^2 + l^2}$. This solution is commonly referred to as the SV spacetime or Schwarzschild spacetime with a black bounce [9]. Subsequently, electrically charged versions of SV-RN black holes were introduced in the literature [10–12]. Additionally, an extension to the rotating case is presented in [13]. It is noteworthy that the SV spacetime exhibits diverse features, describing regular black holes for length scale parameter values below 2, one-way wormholes or black holes with a null throat at $l = 2$, and traversable wormholes for $l > 2$ [14–16].

The presence of the parameter l introduces uncertainty, as its physical significance remains unknown. It has been suggested that l might encapsulate effects arising from quantum gravity [17,18] or be influenced by non-electric or massive scalar fields. Analogous and generalized versions of the SV-black-hole solution are explored in [19], providing an in-depth analysis of the energy conditions within various models [15,17,20].

Hence, to decipher the nature and gravitational implications of the parameter l , one can scrutinize the astrophysical consequences of the (charged/rotating) SV spacetime through observational means. In our prior investigation [21], we delved into the study of Quasi-Periodic Oscillations (QPOs) originating from charged particles orbiting around a magnetized SV spacetime. Our findings indicated that in SV spacetime with magnetic interaction effects, an increase in the l parameter leads to a greater divergence from observed data. This suggests that in microquasars, the central object might manifest as a wormhole rather than a black hole, particularly when the magnetic parameter is elevated.

Additionally, recent work by the authors in [22] explored the shadow characteristics of SV black holes/wormholes, establishing meaningful constraints on the parameter l using data from the Event Horizon Telescope (EHT) observations of the M87* and SgrA* supermassive black holes. Their results demonstrated that the SV black hole's shadow closely resembles that of the Kerr black hole. However, the SV wormhole, being a no-horizon spacetime, can exhibit a closed photon ring when it has substantial spin. The exploration of gravitational lensing/retrolensing in a weak-field limit, alongside investigations into quasi-normal spectra and gray-body factors, has been conducted in the context of the SV spacetime. This research has recently been documented in references [23–25], and the strong deflection limit in the SV spacetime is specifically addressed in Ref. [26,27]. In particular, it has been observed that the photonsphere in the SV spacetime remains independent of the parameter l within the range $l \leq 3$. This finding suggests that the SV metric does not distinguish between a black hole and a wormhole in this parameter range.

Furthermore, in the work presented in Ref. [28], the authors demonstrated that a degeneracy in the combined effects of the black-hole charge and bounce parameters can result in orbital motion around RN SV black holes that is indistinguishable from motion around a Schwarzschild black hole. Additionally, relationships between the black-hole charge and bounce parameter were identified, which have the potential to break this degeneracy. These relationships were derived by utilizing precession data from the S2 star orbits around Sgr A* anchored in the center of the Milky Way galaxy, as detected by the GRAVITY collaboration, and the measured shadow size of the Sgr A* supermassive black hole imaged by the Event Horizon Telescope.

To investigate the structure of spacetime around the RN black hole, one can examine the motion of test particles, as discussed in various studies [29–40]. The characteristics of the RN solution and the influence of the electromagnetic field on the spacetime structure around compact objects are examined in the references (see, e.g., [41–44]).

The presence of external electromagnetic fields surrounding black holes or the intrinsic magnetic fields of the highly magnetized neutron stars significantly impacts rich astronomical observations of compact gravitational objects through electromagnetic radiation. Additionally, it plays a crucial role in influencing the highly energetic astrophysical processes occurring in their vicinity. While an external test electromagnetic field with a magnitude less than 10^{19} G may not alter the spacetime structure, its influence on the

energetic processes and dynamics of charged and magnetized particles around compact gravitational objects is vital [45]. The no-hair theorem posits that black holes cannot possess an intrinsic magnetic field traced to their origin [46]. One approach to investigating magnetic fields associated with black holes involves exploring the external magnetic field in their vicinity. Pioneering work in this area was conducted by R. Wald, particularly in the study of the structure of external electric and magnetic fields around rotating and static black holes immersed in an external asymptotically uniform magnetic field [47].

Over the years, various aspects of electromagnetic field properties near black holes immersed in external asymptotically uniform magnetic fields, as well as the intrinsic magnetic fields of rotating magnetized neutron stars characterized mainly by a dipolar structure, have been extensively examined by multiple researchers across different gravity models [48–50].

In the present paper, we investigate the circular motion and electromagnetic radiation of charged particles near electrically charged black holes in RN SV spacetime. The paper consists of the introduction, four main sections (Sections 2–5), where we discuss the effects of the black hole’s total charge and the black-bounce parameters on the circular motion and radiation of charged particles, and finally, Section 6.

We adopt the spacetime signature $(-, +, +, +)$ and employ the geometrized unit system with $G_N = c = 1$. The Latin indices are anticipated to range from 1 to 3, while the Greek indices span from 0 to 3.

2. Charged Black-Bounce Black holes

The geometry of spacetime around charged (RN) black-bounce black holes can be described using spherical coordinates $(x^\alpha = t, r, \theta, \phi)$ in the following form [11]:

$$ds^2 = -f(r)dt^2 + \frac{dr^2}{f(r)} + h(r)d\Omega_2^2, \quad (1)$$

where the metric components of the “regularized” charged spacetime (for details, see [11]) are

$$f(r) = 1 - \frac{2M}{\sqrt{r^2 + l^2}} + \frac{Q^2}{r^2 + l^2}; \quad h(r) = r^2 + l^2, \quad (2)$$

The event horizon radius can be found by solving $f(r) = 0$, as follows:

$$\frac{r}{M} = \sqrt{2 \left(1 + \sqrt{1 - \frac{Q^2}{M^2}} \right) - \frac{l^2 - Q^2}{M^2}}. \quad (3)$$

We visually examine the characteristics of the event horizon in Figure 1. Notably, when $Q = 0$, the event horizon becomes zero at $l = 2$, resulting in the transformation (coincidence) of the black-hole spacetime into a wormhole spacetime. However, this limit diminishes to $l = 1$ for the maximum value of the black-hole charge $Q = 1$. Likewise, the maximum value of Q also decreases with the increase in l .

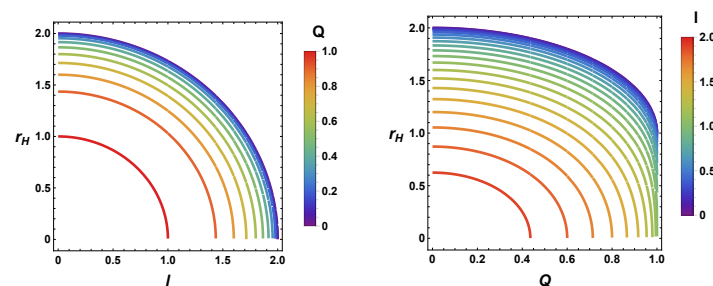


Figure 1. The event horizon radius vs. the black-hole charge and the length parameter. $M = 1$.

The strength of the electric field around the charged SV black hole is [11]

$$E(r) = \frac{Qr}{(r^2 + l^2)^{3/2}}. \quad (4)$$

One can find the time component of the electromagnetic four-potentials by integrating $A_t = \int E(r)dr$, and we have

$$A_t = -\frac{Q}{\sqrt{r^2 + l^2}}. \quad (5)$$

3. Charged-Particle Motion

In this section, we analyze the motion of charged particles characterized by mass m and electric charge e moving within the combined gravitational and electromagnetic fields specified by the lapse function in Equation (2) and the four-potential electromagnetic vector outlined in Equation (5).

3.1. Equations of Motion for Charged Particles

In this section, we derive equations of motion of charged particles in circular orbits in spacetime (1) using the Hamilton–Jacobi equation,

$$g^{\mu\nu} \left(\frac{\partial \mathcal{S}}{\partial x^\mu} - eA_\mu \right) \left(\frac{\partial \mathcal{S}}{\partial x^\nu} - eA_\nu \right) = -m^2. \quad (6)$$

The action of charged particles' motion has the following separated form:

$$\mathcal{S} = -Et + L\phi + S_r + S_\theta. \quad (7)$$

Here, E and L are integrals of motion defining the energy and angular momentum of the charged particle, respectively. S_r and S_θ are the radial and angular functions. After some algebraic calculations, one can obtain

$$-\frac{1}{f(r)}(E - eA_t)^2 + f(r) \left(\frac{\partial S_r}{\partial r} \right)^2 + \frac{1}{h(r)} \left(\frac{\partial S_\theta}{\partial \theta} \right)^2 + \frac{L^2}{h(r) \sin^2 \theta} = -m^2. \quad (8)$$

From this point, we restrict the motion of the particle to a constant plane $\theta = \theta_0$, without vertical motion $\dot{\theta} = 0$ ($p_\theta = (\partial S_\theta / \partial \theta) \equiv 0$), and we have

$$\dot{t} = \frac{1}{f(r)} (\mathcal{E} - qA_t), \quad (9)$$

$$\dot{\phi} = \frac{\mathcal{L}}{h(r) \sin^2 \theta_0}, \quad (10)$$

$$\dot{r}^2 = (\mathcal{E} - qA_t)^2 - f(r) \left(1 + \frac{\mathcal{L}^2}{h(r) \sin^2 \theta_0} \right) \quad (11)$$

where $q = e/m$ is the specific charge of the particles, and $\mathcal{E} = E/m$ and $\mathcal{L} = L/m$ are the specific energy and angular momentum of the particles, respectively, known as integrals of motion. One can rewrite the equation for the radial motion at the fixed plane in the standard form,

$$\dot{r}^2 = (\mathcal{E} - V_{\text{eff}}^-) (\mathcal{E} - V_{\text{eff}}^+). \quad (12)$$

The circular motion of the charged particles can be described using the equations $\mathcal{E} = V_{\text{eff}}$ and $\dot{r} = 0$, and the effective potential can be found as solutions of Equation (11).

Hence, the effective potential for the circular motion of the charged particles reads in the equatorial plane ($\theta_0 = \pi/2$) as

$$V_{\text{eff}}^{\pm}(r; \mathcal{L}) = qA_t \pm \sqrt{f(r) \left(1 + \frac{\mathcal{L}^2}{h(r)} \right)}. \quad (13)$$

The effective potential is composed of two components, namely Coulomb and gravitational interactions, and exhibits symmetry dependent on the sign of q , which represents the specific charge of the test particle. Throughout the paper, we consistently refer to the effective potential as V_{eff}^+ , unless explicitly stated otherwise [51].

In our investigation, we specifically consider the positive root of the effective potential, denoted by V_{eff}^+ . This choice corresponds to what is known as positive root states, where the four-velocity is oriented toward the future and the energy is positive relative to local observers. For a more in-depth understanding, see [46].

In Figure 2, we illustrate the radial variations in the effective potential $V_{\text{eff}} = V^+$ for different combinations of black hole and particle charges, as well as length parameters. In this examination, we maintain the angular momentum at a fixed value of $\mathcal{L}^2/M^2 = 20$. The gravitational influence of the RN black hole charge is observed to increase the maximum effective potential. However, for positive values of the qQ coupling and the l parameter, the maximum decreases, while, for $qQ < 0$, the effective potential increases.

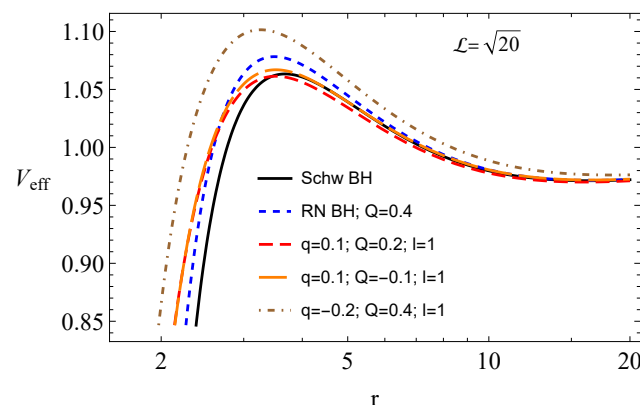


Figure 2. Radial profiles of the effective potential for the circular motion of charged particles around RN SV black holes. $M = 1$.

3.2. Circular Orbits

The solutions of $V'_{\text{eff}} = 0$ (where $'$ indicates a partial derivative by r) within the fixed background indicate that a particle with a particular specific charge q traces a circular orbit at a specified radius r when its specific angular momentum satisfies the corresponding relation:

$$\mathcal{L}_{\pm}^2 = \frac{1}{[h(r)f'(r) - f(r)h'(r)]^2} \left\{ f(r)h^2(r)f'(r)h'(r) - h^3(r)(f'(r)^2 - 2f(r)qA'(r)^2) \right. \\ \left. \pm qA'(r)f(r)h^2(r)\sqrt{h^2(r)q^2A'(r)^2 - h'(r)[h(r)f'(r) - f(r)h'(r)]} \right\}. \quad (14)$$

When $Q = 0$ and $l = 0$, corresponding to the Schwarzschild case, the angular momentum solution for circular orbits can be expressed as $\mathcal{L}_{\pm}^2 = Mr^2/(r - 3M)$. Now, we will investigate the solution in (14) to identify the conditions under which both \mathcal{L}_{\pm}^2 are real.

For the solution in Equation (14) to produce real values, the expression under the square root must remain consistently positive. Therefore, when considering the specific angular momentum at the circular orbit, we need to consider two scenarios:

- Since $h^2(r)q^2A'(r)^2$ is always positive, $h(r)f'(r) - f(r)h'(r) \leq 0$ must be found for any specific charge q and for $q = 0$;
- When $h(r)f'(r) - f(r)h'(r) > 0$, then $h^2(r)q^2A'(r)^2 \geq h'(r)|h(r)f'(r) - f(r)h'(r)|$ must be satisfied for large values of the particle's charge.

One can see from Equation (14) that $\mathcal{L}_+^2 < \mathcal{L}_-^2$ for positive charges and $\mathcal{L}_-^2 > \mathcal{L}_+^2$ for negatively charged particles. Therefore, $\mathcal{L}_+^2|_{q<0} = \mathcal{L}_-^2(q > 0) < \mathcal{L}_+^2(q > 0) = \mathcal{L}_-^2(q < 0)$.

The conditions outlined in (15) require establishing stable circular orbits, implying a balance between competing forces that act on the charged particle. Three forces, Coulomb, gravitational, and centrifugal, act on the particle during its orbit around the charged black-bounce black hole. For negatively charged particles, gravitational and Coulomb forces align in the same direction, while the centrifugal force points inward toward the charged black hole with $Q > 0$. To maintain equilibrium, the sum of Coulomb and gravitational forces must counteract the centrifugal one. This involves using \mathcal{L}_-^2 for negatively charged particles, considering that the centrifugal force is proportional to \mathcal{L}^2 , and the value of \mathcal{L}^2 should be large enough to prevent the particle from falling into the central object.

On the contrary, for positively charged particles, both the centrifugal and Coulomb forces are in the same direction. Therefore, for positively charged particles, we exclusively employ \mathcal{L}_-^2 since the value of \mathcal{L}^2 should be small enough to prevent the particle from being pulled to infinity. Given these considerations, we examine the radii of the circular orbits of charged particles using the solution \mathcal{L}_-^2 obtained from Equation (14), where $r > r_{crit}$, where r_{crit} is the radius of the last circular orbit.

The radial profiles of the angular momentum and energy of charged particles are depicted in Figure 3 for circular orbits in the spacetime of an electrically charged RN SV black hole, considering various values of the parameters q , Q , and l . In the top-left panel, it is evident that both the gravitational influence of the black-hole charge and the Coulomb forces contribute to a reduction in the values of angular momentum and energy. Similarly, the impact of the parameter l also leads to a decrease in both quantities.

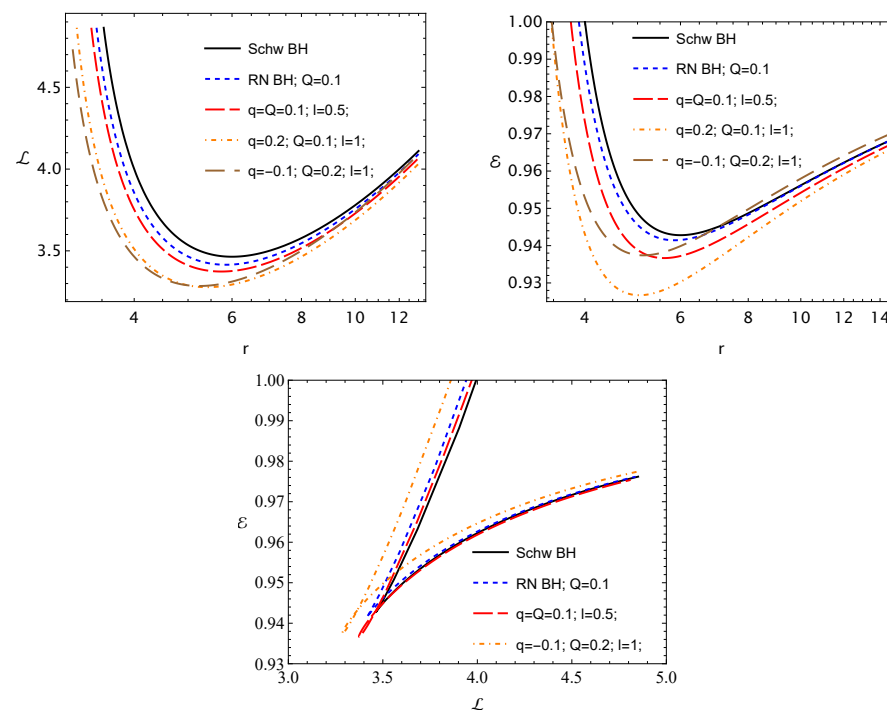


Figure 3. The angular momentum (top left) and energy (top right) of charged particles for circular orbits as a function of the radial coordinate. The (bottom panel) represents $\mathcal{E} - \mathcal{L}$ space for different l , q , and Q parameters, and $M = 1$.

3.3. Charged-Particle Trajectories

In Figures 4 and 5, we demonstrate the trajectories of positively ($q = 1$) and negatively ($q = -1$) charged particles in the spacetime of charged black-bounce black holes ($Q = 0.2$), respectively. Here, we use the initial conditions for the angular momentum of the particles $\mathcal{L} = 3$, with initial radial and angular coordinates $r_0 = 7$ and $\theta_0 = (\pi/2 + 0.2)$ rad, respectively. We have examined the values of the parameter $l = 1, 1.7$, and 1.8 . It is observed from the figures that the parameter l weakens gravity near the black hole. One can see that the positively charged particles fall into the black hole at $l = 1.7$. However, under the same conditions, negatively charged particles have some bounded orbits. In the case of $l = 1.8$, the particles with $q = 1$ orbit in bounded orbits that differ from the orbits of the particles with $q = -1$.

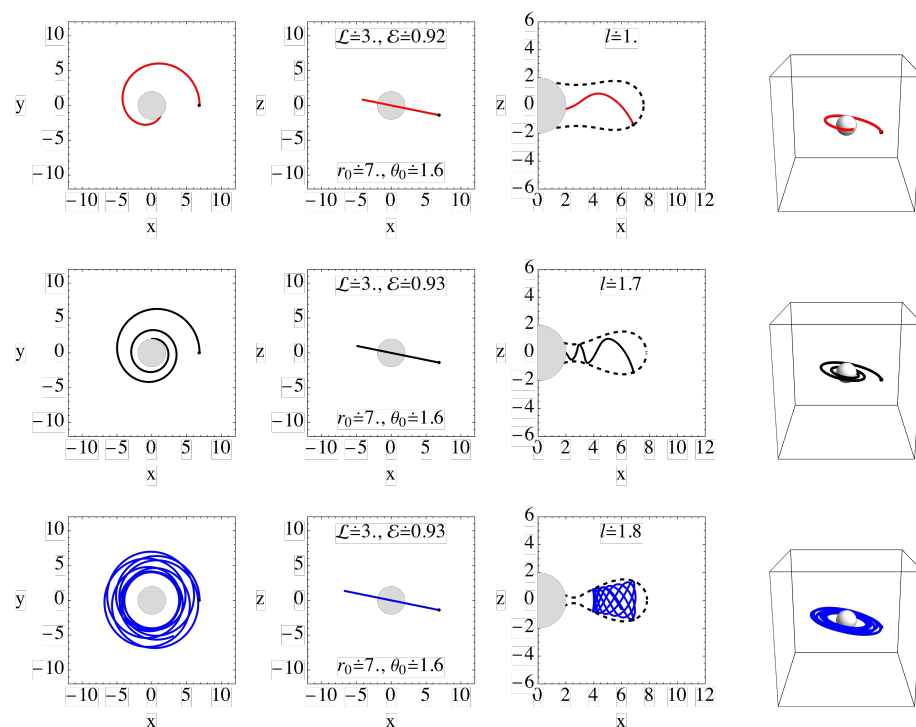


Figure 4. Trajectories of positively charged particles around the charged black-bounce RN black holes for different values of l . Here, we fixed $\mathcal{L} = 0.3, q = 1, Q = 0.2, M = 1$, and initial coordinates are taken as $r_0 = 7$ & $\theta = 1.6(\pi/2 + 0.2)$ rad.

3.4. The ISCO Radius

Presently, we investigate the ISCOs of charged particles revolving around charged black holes within the SV spacetime. From an astrophysical standpoint, ISCOs serve to delineate the inner boundary of the accretion disk encircling the black hole. The stability of circular orbits in a fixed plane is determined by meeting the following conditions:

$$V_{\text{eff}} = \mathcal{E}, \quad V'_{\text{eff}} = 0, \quad V''_{\text{eff}} \geq 0. \tag{15}$$

Here, we examine the impact of particle and black-hole charges, along with the length parameters, on the ISCO radius.

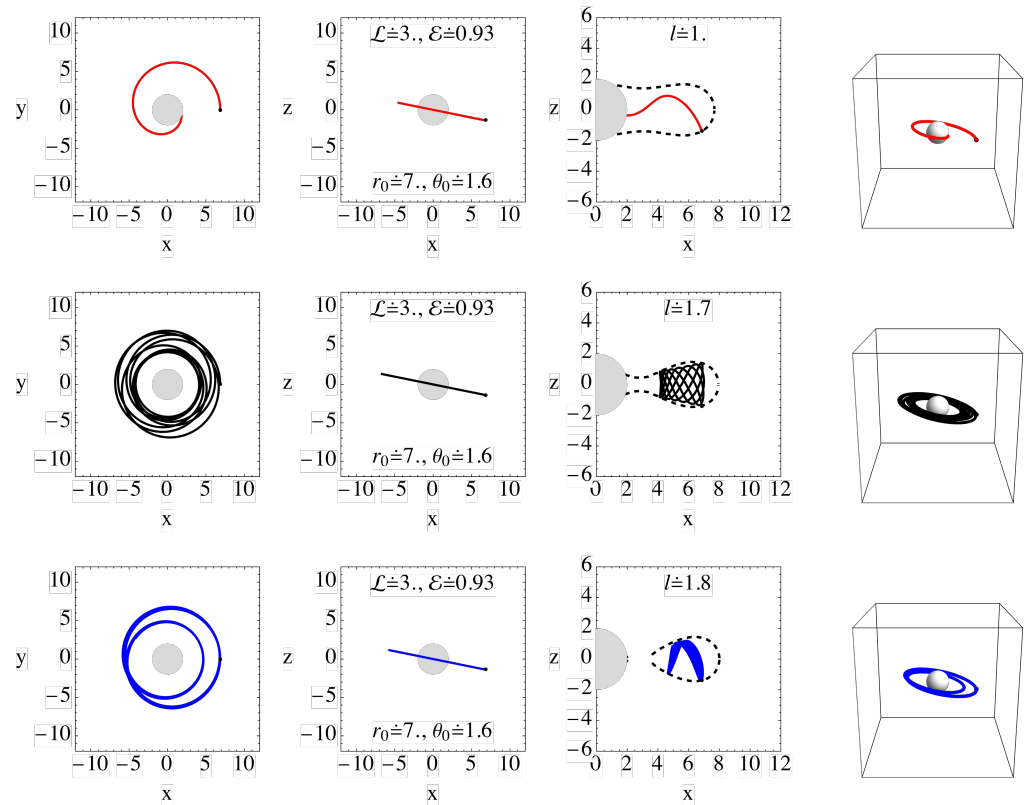


Figure 5. The same figure as Figure 4, but for negatively charged particles. In this case, we also fixed $\mathcal{L} = 0.3$, $q = 1$, $Q = 0.2$, $M = 1$, and initial coordinates are taken as $r_0 = 7$ & $\theta = 1.6(\pi/2 + 0.2)$ rad.

In Figure 6, we illustrate the relationship between the ISCO radius of charged particles and their charge (top row), the black-hole charge (bottom right panel), and the parameter l . In particular, there is a symmetric behavior in ISCO profiles when q is replaced by $-q$ and $-Q$ is replaced by Q , that is, $qQ \rightarrow -qQ$. For $Q = 0.1$ ($Q = -0.1$), a minimum in the ISCO value is observed at $r_{ISCO} = 5.97744$ for $q = -0.05$ ($q = 0.05$), and when $Q = \pm 0.2$, the ISCO minimum changes to $r_{ISCO} = 5.8546$ at $q = \pm 0.1$. The increase in l leads to a decrease in the ISCO radius, ultimately reaching zero at a critical value of l that defines the wormhole spacetime.

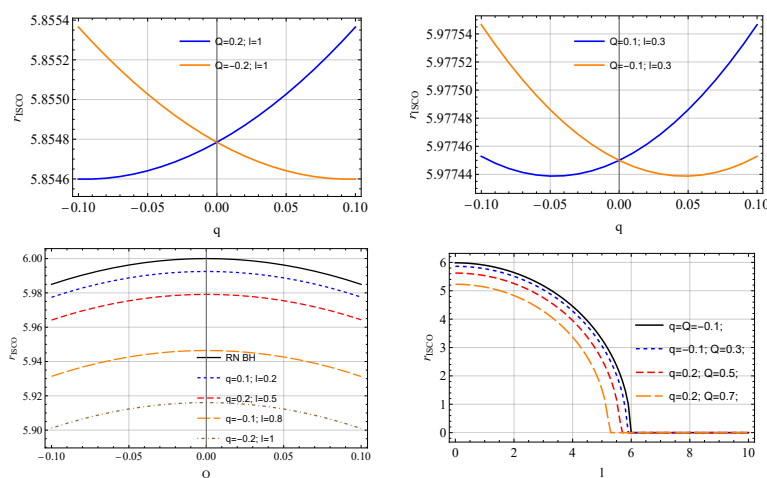


Figure 6. ISCO profiles: The dependence of the ISCO radius on the particle charge (top two panels) for $Q = \pm 0.2$ (left panel) and $Q = \pm 0.1$ (right panel); ISCO radius vs. the black hole (left-bottom panel); ISCO radius vs. l parameter (bottom-right panel). $M = 1$.

3.5. Angular Momentum at ISCO

In this subsection, we discuss the angular momentum of charged particles at their ISCOs around the charged black-bounce black hole.

Examining Figure 7, it is evident that for electrically neutral particles, the angular momentum (\mathcal{L}_{ISCO}) experiences a symmetric and slight decrease in both negative and positive values of Q . Conversely, in the case of $Q > 0$, the angular momentum increases (decreases) for positively (negatively) charged particles. However, all results exhibit the inverse behavior when $Q < 0$. Thus, symmetrically inverse results can be observed when the coupling parameter qQ approaches its negative counterpart, denoted as $-qQ$.

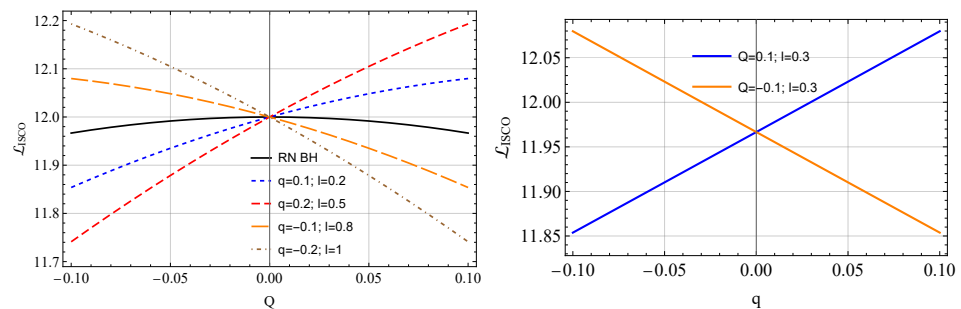


Figure 7. Values of angular momentum of charged particles corresponding to ISCOs around charged black-bounce black holes versus the black-hole charge Q (left panel), and the particle's charge (right panel). $M = 1$.

3.6. Energy at ISCO

In this context, we explore the impact of charge variations on the energy of charged particles around the charged bouncing black hole at their ISCOs, considering variations in both black-hole and particle charges, as well as the parameter l .

The patterns in the ISCO energy profiles, as evident in Figure 8, closely resemble the trends observed in the angular momentum profiles presented in Figure 7 for neutral particles. However, in the scenario where $qQ < 0$, the energy \mathcal{E} experiences an increase, whereas for $qQ > 0$, it decreases in a (quasi)linear fashion. It should be noted that even slight variations in the values of q and Q lead to significant changes in both \mathcal{L}_{ISCO} and \mathcal{E}_{ISCO} . Furthermore, a marginal increase in l results in a slight reduction in both the energy and angular momentum.

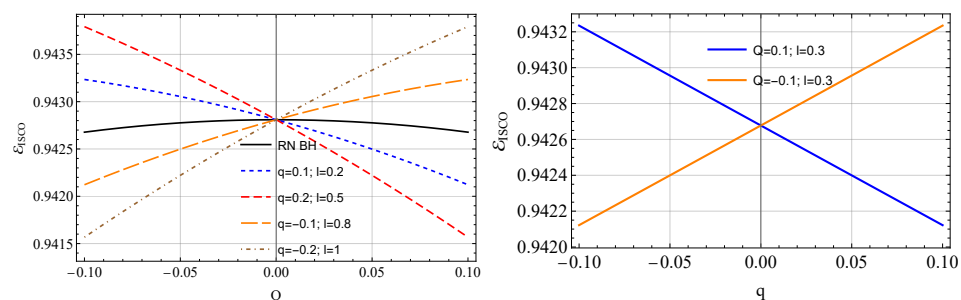


Figure 8. Similar figure to Figure 7, but for the particle energy at ISCOs. $M = 1$.

The connections between the ISCO energy and the ISCO angular momentum are depicted in Figure 9 across various configurations of black-hole and particle charges, as well as the parameter l . The figure reveals that particles can exhibit a correspondingly large ISCO energy and ISCO angular momentum, with notably greater energy in cases of electric repulsion, when $qQ < 0$, compared to instances of electric attraction ($qQ > 0$).

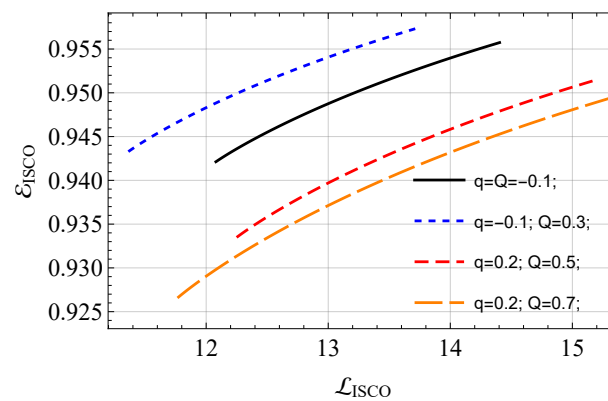


Figure 9. The angular momentum vs. energy of the particles at their ISCOs around the RN black hole in SV spacetime. $M = 1$.

4. The Energy Efficiency

A compelling scenario unfolds when examining the dynamics of a charged test particle within a Keplerian accretion disk as it descends toward the central black hole, releasing energy in the form of electromagnetic and/or gravitational radiation. The quantity of radiated energy is determined by the contrast between the particle's locally observed rest energy and its energy at the ISCO, acting as a reflection of the spacetime characteristics. Consequently, the energy efficiency of the accretion disk can be calculated using the formula introduced by Novikov in 1973 [52].

The significance of the ISCO in the vicinity of black holes is associated with the inner boundary of an accretion disk. Intriguingly, as test particles plunge into the central region of the black hole within the Keplerian accretion disk, they extract a specific amount of energy that may be converted into electromagnetic and gravitational radiation under certain constraints. The energy released through radiation is commonly computed as the difference between the particle's rest energy (as determined by a suitable observer) and the particle's ISCO energy ($\mathcal{E}_{\text{ISCO}}$) [52].

According to [53], electromagnetic radiation in an accretion disk is due to the rotational kinetic energy of the disk, and it is mainly dependent on the rate of matter inflow. In fact, the physics of the accretion disk is more complicated than we know, and there are lots of factors one has to take into account when studying the dynamics of the steady accretion disk, such as the role of viscosity, radiation mechanisms, time dependence, instability, variability, the inner boundary, etc. [54].

Moreover, the bolometric luminosity emitted from the accretion disk is directly correlated with the energy efficiency of the central black hole, expressed by the equation $\eta = L_{\text{bol}}/(\dot{M}c^2)$, where \dot{M} denotes the accretion rate [55].

In this context, here, we also explore the efficiency of released energy, taking into account the electromagnetic forces acting on electrically charged particles by the electric field generated by the electric charge of the black-bounce RN black hole. Consequently, the efficiency of the energy released from the accretion disk can be mathematically represented as follows [52]:

$$\eta = 1 - \mathcal{E} \Big|_{r=r_{\text{ISCO}}} . \quad (16)$$

The impact of the Coulomb interaction between the electric charges of the black hole and the particles orbiting the black-bounce RN black hole on the efficiency of energy release from the accretion disk is illustrated in Figure 10 for various values of l . The efficiency of energy release increases with increasing positive values of the qQ coupling, while it decreases when qQ is negative. For the scenario where $q = 0$ (depicted by the black line in the left panel and referred to as RN BH), both positive and negative values of the black-hole charge lead to a slight increase in efficiency.

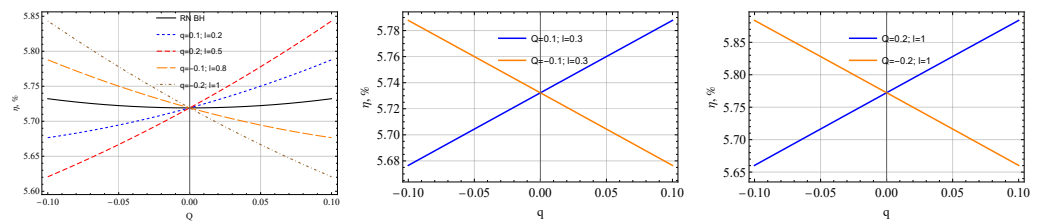


Figure 10. The dependence of the energy efficiency on the black-hole and particle charges $M = 1$.

5. Intensity of Electromagnetic Radiation by Accelerated Charged Particle

The process of matter accretion around both supermassive and stellar-mass black holes is widely acknowledged as a mechanism for producing high-energy relativistic particles near active galactic nuclei and the low-mass X-ray binary sources associated with stars, respectively. Although the precise mechanisms governing the generation of energy in these highly energetic sources remain to be fully understood, there is a prevalent consensus that underscores the substantial influence of magnetic fields in the surroundings of rotating black holes, playing a crucial role in the creation of high-energy relativistic particles [56–58].

An essential inquiry arises concerning the relevance of a black hole’s charge in the context of extracting energy. It is firmly established that relativistic charged particles, particularly those propelled by an external electromagnetic field, release electromagnetic radiation. Synchrotron radiation from an accelerated charged particle, a fundamental example of such radiation processes, serves as a relativistic variant of cyclotron radiation. Prior investigations have explored synchrotron radiation from charged particles near a magnetized Schwarzschild black hole (Landau and Lifshitz, 2013) [59]. One may determine the ISCO radius, being the inner edge of the accretion disk around a black hole, through iron emission lines in the accretion disk [60], X-ray reverberation around the black hole [61], and the energetic spectrum of relativistic jets [62], which may help to determine the black-hole spin.

In this context, our focus shifts to the exploration of electromagnetic radiation emitted by an accelerated charged particle orbiting around a charged black hole. The radiation spectrum produced by a relativistic charged particle in profoundly curved spacetime is expressed as (see Ref. [63] for details),

$$I = \frac{2q^2}{3} w_\alpha w^\alpha, \tag{17}$$

where $w^\alpha = U^\beta \nabla_\beta U^\alpha$, and it stands for the four-acceleration. Using the non-geodesic equation, it is expressed as

$$\frac{dU^\alpha}{d\lambda} + \Gamma_{\mu\nu}^\alpha U^\mu U^\nu = \frac{q}{m} F^\alpha_\beta U^\beta, \tag{18}$$

We can rewrite the expression for the four-acceleration of the charged particles in an external electromagnetic field in the following form:

$$w^\alpha = \frac{q}{m} F^\alpha_\beta U^\beta, \quad w_\alpha U^\alpha \equiv 0. \tag{19}$$

As evident from Equation (19), the four accelerations of the particle are perpendicular to its four velocities. In conclusion, considering all the previously discussed points, the formulation for the spectrum of electromagnetic radiation can be expressed as [63]

$$I = \frac{2q^4}{3m^2} F_{\alpha\gamma} F^{\gamma\beta} U^\alpha U_\beta. \tag{20}$$

5.1. Acceleration of Charged Particles in Stable Circular Orbits

In this case, we assume that charged particles radiate in stable circular orbits in a fixed plane $U^\alpha = U^t(1, 0, 0, \Omega)$, where $\Omega = \frac{d\phi}{dt}$ is the angular velocity of the particles. The directions of the velocity and acceleration of the charged particles are perpendicular, satisfying the condition $w_\alpha U^\alpha \equiv 0$, and we have $w^\alpha = (0, w^r, 0, 0)$, with

$$w_r = \frac{qE_{rt}}{m\sqrt{-g_{tt} - \Omega^2 g_{\phi\phi}}} \tag{21}$$

Using Equations (20) and (21), one may obtain an estimation of the intensity [63]:

$$I \simeq 1.3 \times 10^{24} \left(\frac{q}{e}\right)^4 \left(\frac{m_e}{m}\right)^2 \left(\frac{M_\odot}{M}\right)^2 \left(\frac{f}{f - \Omega^2 r^2}\right)^2, \tag{22}$$

To show the effect of l , below, we analyze the intensity (22), normalizing it to the RN-black-hole case.

Graphical analyses of the ratio of the intensity of the radiation of charged test particles ($q = 1$ and $q = -1$) in circular orbits around charged black-bounce black holes and RN black holes $I(r, l, Q, q)/I(r, 0, Q, q)$ are presented in Figure 11, with the left and right panels showing the $Q > 0$ and $Q < 0$ cases, respectively. The intensity decreases with increasing l , as well as in the case of $qQ > 0$. However, it increases in $qQ < 0$ cases. The intensity rate is higher in the $qQ < 0$ case than in $qQ > 0$ at larger values of l .

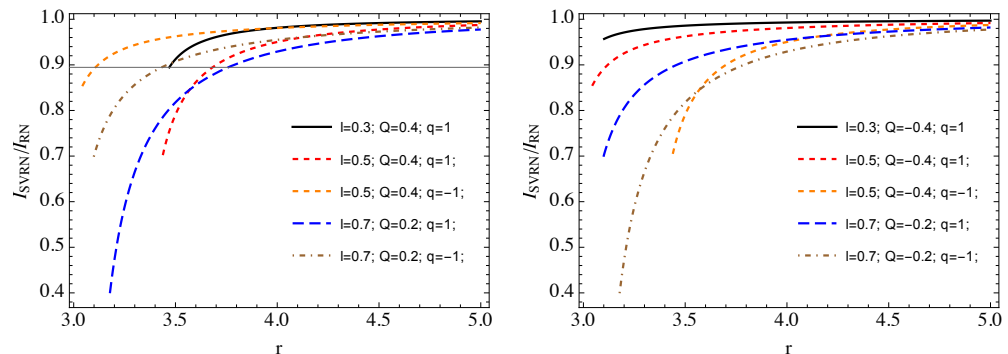


Figure 11. Radial dependence of the intensity of electromagnetic radiation of charged particles orbiting the black-bounce RN black hole along circular orbits normalized to the RN limit at $l = 0$ for various values of the parameters q, Q (left and right panels for $Q > 0$ and $Q < 0$ cases, respectively), and l . $M = 1$.

5.2. Acceleration of Falling Charged Particles into Central Black Hole

In this subsection, we assume that the charged particles are falling, with spiral-like trajectories, into the central charged black hole with the four-velocity $U^\alpha = U^t(1, u, 0, \Omega)$ ($u = \frac{dr}{dt}$ is the radial velocity) and the corresponding four-acceleration $w^\alpha = (w^t, w^r, 0, 0)$ (where $w_t = \frac{q}{m} F_{tr} U^r$ and $w_r = \frac{q}{m} F_{rt} U^t$). Consequently, one can obtain the expression of the intensity of electromagnetic radiation by falling charged particles in this form [63]:

$$I = -\frac{2q^4}{3m^2} \left(\frac{u^2 g^{tt} + g^{rr}}{g_{tt} + u^2 g_{rr} + \Omega^2 g_{\phi\phi}} \right) F_{rt}^2. \tag{23}$$

In Figure 12, we show the radial profiles of the intensity of charged particles falling into the charged RN SV black hole normalized to the RN limit ($l = 0$) for positive (left panel) and negative (right panel) values of Q . One can see that the presence of l causes a decrease in the intensity. Also, the intensity rates are almost the same at larger values of

l and smaller values of qQ . However, at smaller l and larger qQ , the intensity is slightly greater in the case $qQ > 0$ than in $qQ < 0$.

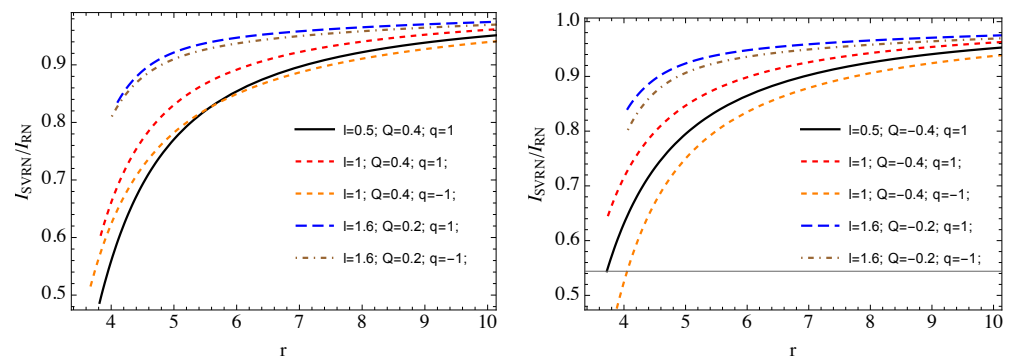


Figure 12. Similar figure to Figure 11, but for the radiation of falling charged particles (left and right panels for $Q > 0$ and $Q < 0$ cases, respectively). $M = 1$.

6. Conclusions

In this study, we investigated the circular orbits of electrically charged particles around electrically charged black-bounce RN black holes, known as RN SV black holes.

- First, we have analyzed the effective potential for circular orbits and found that the gravitational effect of the RN black hole's charge increases the maximum of the effective potential. However, for positive values of the qQ coupling and the l parameter, the maximum decreases, while, for $qQ < 0$, the effective potential increases.
- Also, we have studied the circular orbits of charged particles and shown that both the gravitational influence of the black-hole charge and the Coulomb forces contribute to a reduction in the values of angular momentum and energy corresponding to circular orbits. Similarly, the impact of the parameter l also leads to a decrease in both quantities.
- It is also shown that there is a symmetrical behavior in ISCO profiles when q is replaced by $-q$ and $-Q$ is replaced by Q , i.e., $qQ \rightarrow -qQ$. For $Q = 0.1$ ($Q = -0.1$), a minimum in the ISCO values is observed at $r_{ISCO} = 5.97744$ for $q = -0.05$ ($q = 0.05$), and when $Q = \pm 0.2$, the ISCO minimum changes to $r_{ISCO} = 5.8546$ at $q = \pm 0.1$. The increase in l leads to a decrease in the ISCO radius, ultimately reaching zero at a critical value of l that defines the wormhole spacetime.
- Our performed analyses have shown that the angular momentum (\mathcal{L}_{ISCO}) for electrically neutral particles slightly decreases for both negative and positive values of Q . Conversely, in the case of $Q > 0$, the angular momentum increases (decreases) for positively (negatively) charged particles.
- In a similar scenario, for $qQ < 0$, the energy \mathcal{E} increases, while for $qQ > 0$, it decreases in a (quasi)linear fashion. It is worth noting that even small variations in the values of q and Q lead to significant changes in both \mathcal{L}_{ISCO} and \mathcal{E}_{ISCO} . Furthermore, a marginal increase in l results in a slight reduction in both the energy and angular momentum.

Finally, we have investigated the intensity of the radiation of charged particles orbiting along circular orbits and falling into the central charged RN black hole in the SV spacetime, leading to the following observations:

- In the case of the radiation from orbiting charged particles, the intensity of the radiation decreases with increasing l , as well as in the case of $qQ > 0$. However, it increases in $qQ < 0$ cases.
- In the case of falling charged particles, the effect of the l parameter is long-lasting at far distances. The intensity rates are almost the same at higher values of l and lower values of qQ . However, for a smaller l and a bigger qQ , the intensity is slightly larger in the $qQ > 0$ case than in the $qQ < 0$ one.

Author Contributions: The roles and contributions of the authors for this work are as follows: Conceptualization: J.R. and S.M.; Methodology: J.R. and K.B.; Software: J.R., S.M. and K.B.; Validation: B.A. and Z.S.; Formal Analysis: J.R., B.A., S.M. and K.B.; Investigation: B.A., Z.S. and K.B. All authors have reviewed and approved the final version of the manuscript for publication.

Funding: Grants from the Ministry of Higher Education, Science, and Innovation of the Republic of Uzbekistan: FZ-20200929385, F-FA-2021-432, F-FA-2021-510, and MRB-2021-527.

Data Availability Statement: Data are contained within the article.

Acknowledgments: S.M. gratefully acknowledges the Carl von Ossietzky University of Oldenburg in Germany for its hospitality. J.R. acknowledges the Silesian University in Opava for its hospitality.

Conflicts of Interest: The authors declare no conflicts of interest.

References

1. Reissner, H. Über die Eigengravitation des elektrischen Feldes nach der Einsteinschen Theorie. *Ann. Phys.* **1916**, *355*, 106–120. [[CrossRef](#)]
2. Nordström, G. On the Energy of the Gravitation field in Einstein's Theory. *K. Ned. Akad. Wet. Proc. Ser. Phys. Sci.* **1918**, *20*, 1238–1245.
3. Bardeen, J.M. Non-singular general-relativistic gravitational collapse, In Proceedings of the 5th International Conference on Gravitation and the Theory of Relativity, Tbilisi, Georgia, 9–16 September 1968; DeWitt, C., DeWitt, B., Eds.; Gordon and Breach: Tbilisi, Georgia, 1968; p. 174.
4. Ayón-Beato, E.; García, A. Regular Black Hole in General Relativity Coupled to Nonlinear Electrodynamics. *Phys. Rev. Lett.* **1998**, *80*, 5056–5059. [[CrossRef](#)]
5. Ayon-Beato, E. New regular black hole solution from nonlinear electrodynamics. *Phys. Lett. B* **1999**, *464*, 25–29. [[CrossRef](#)]
6. Ayon-Beato, E.; Garcia, A. Non-Singular Charged Black Hole Solution for Non-Linear Source. *Gen. Relativ. Gravit.* **1999**, *31*, 629. [[CrossRef](#)]
7. Bronnikov, K.A. Regular magnetic black holes and monopoles from nonlinear electrodynamics. *Phys. Rev. D* **2001**, *63*, 044005. [[CrossRef](#)]
8. Bambi, C.; Modesto, L. Rotating regular black holes. *Phys. Lett. B* **2013**, *721*, 329–334. [[CrossRef](#)]
9. Simpson, A.; Visser, M. Black-bounce to traversable wormhole. *J. Cosmol. Astropart. Phys.* **2019**, *2019*, 042. [[CrossRef](#)]
10. Cañate, P. Black bounces as magnetically charged phantom regular black holes in Einstein-nonlinear electrodynamics gravity coupled to a self-interacting scalar field. *Phys. Rev. D* **2022**, *106*, 024031. [[CrossRef](#)]
11. Franzin, E.; Liberati, S.; Mazza, J.; Simpson, A.; Visser, M. Charged black-bounce spacetimes. *J. Cosmol. Astropart. Phys.* **2021**, *2021*, 036. [[CrossRef](#)]
12. Bokulić, A.; Smolić, I.; Jurić, T. Constraints on singularity resolution by nonlinear electrodynamics. *Phys. Rev. D* **2022**, *106*, 064020. [[CrossRef](#)]
13. Mazza, J.; Franzin, E.; Liberati, S. A novel family of rotating black hole mimickers. *J. Cosmol. Astropart. Phys.* **2021**, *2021*, 082. [[CrossRef](#)]
14. Lobo, F.S.N.; Rodrigues, M.E.; Silva, M.V.d.S.; Simpson, A.; Visser, M. Novel black-bounce spacetimes: Wormholes, regularity, energy conditions, and causal structure. *Phys. Rev. D* **2021**, *103*, 084052. [[CrossRef](#)]
15. Xu, Z.; Tang, M. Rotating spacetime: Black-bounces and quantum deformed black hole. *Eur. Phys. J. C* **2021**, *81*, 863. [[CrossRef](#)]
16. Churilova, M.S. Quasinormal modes of the Dirac field in the novel 4D Einstein-Gauss-Bonnet gravity. *arXiv* **2020**, arXiv:2004.00513.
17. Bronnikov, K.A. Black bounces, wormholes, and partly phantom scalar fields. *Phys. Rev. D* **2022**, *106*, 064029. [[CrossRef](#)]
18. Fu, Q.M.; Zhang, X. Gravitational lensing by a black hole in effective loop quantum gravity. *Phys. Rev. D* **2022**, *105*, 064020. [[CrossRef](#)]
19. Pal, K.; Pal, K.; Sarkar, T. Analogue Metric in a Black-Bounce Background. *Universe* **2022**, *8*, 197. [[CrossRef](#)]
20. Yang, Y.; Liu, D.; Övgün, A.; Long, Z.W.; Lambiase, G. Rotating black bounces surrounded by the string cloud. *arXiv* **2023**, arXiv:2307.09344. [[CrossRef](#)]
21. Vrba, J.; Rayimbaev, J.; Stuchlik, Z.; Ahmedov, B. Charged particles motion and quasiperiodic oscillation in Simpson-Visser spacetime in the presence of external magnetic fields. *Eur. Phys. J. C* **2023**, *83*, 854. [[CrossRef](#)]
22. Shaikh, R. Testing black hole mimickers with the Event Horizon Telescope image of Sagittarius A*. *Mon. Not. R. Astron. Soc.* **2023**, *523*, 375–384. [[CrossRef](#)]
23. Guo, Y.; Lan, C.; Miao, Y.G. Bounce corrections to gravitational lensing, quasinormal spectral stability and gray-body factors of Reissner-Nordström black holes. *arXiv* **2022**, arXiv:2201.02971. [[CrossRef](#)]
24. Tsukamoto, N. Retrolensing by two photon spheres of a black-bounce spacetime. *Phys. Rev. D* **2022**, *105*, 084036. [[CrossRef](#)]
25. Zhang, J.; Xie, Y. Gravitational lensing by a black-bounce-Reissner-Nordström spacetime. *Eur. Phys. J. C* **2022**, *82*, 471. [[CrossRef](#)]
26. Tsukamoto, N. Gravitational lensing by two photon spheres in a black-bounce spacetime in strong deflection limits. *Phys. Rev. D* **2021**, *104*, 064022. [[CrossRef](#)]

27. Islam, S.U.; Kumar, J.; Ghosh, S.G. Strong gravitational lensing by rotating Simpson-Visser black holes. *J. Cosmol. Astropart. Phys.* **2021**, *2021*, 013. [[CrossRef](#)]
28. Zhang, J.; Xie, Y. Probing a black-bounce-Reissner-Nordström spacetime with precessing and periodic motion. *Eur. Phys. J. C* **2022**, *82*, 854. [[CrossRef](#)]
29. Sharp, N.A. Geodesics in black hole space-time. *Gen. Relativ. Gravit.* **1979**, *10*, 659–670. [[CrossRef](#)]
30. Frolov, V.P.; Novikov, I.D. *Black Hole Physics, Basic Concepts and New Developments*; Kluwer Academic Publishers: Dordrecht, The Netherlands, 1998.
31. Jawad, A.; Ali, F.; Jamil, M.; Debnath, U. Dynamics of Particles Around a Regular Black Hole with Nonlinear Electrodynamics. *Commun. Theor. Phys.* **2016**, *66*, 509. [[CrossRef](#)]
32. Hussain, S.; Jamil, M. Timelike geodesics of a modified gravity black hole immersed in an axially symmetric magnetic field. *Phys. Rev. D* **2015**, *92*, 043008. [[CrossRef](#)]
33. Jamil, M.; Hussain, S.; Majeed, B. Dynamics of particles around a Schwarzschild-like black hole in the presence of quintessence and magnetic field. *Eur. Phys. J. C* **2015**, *75*, 24. [[CrossRef](#)]
34. Hussain, S.; Hussain, I.; Jamil, M. Dynamics of a charged particle around a slowly rotating Kerr black hole immersed in magnetic field. *Eur. Phys. J. C* **2014**, *74*, 210. [[CrossRef](#)]
35. Babar, G.Z.; Jamil, M.; Lim, Y.K. Dynamics of a charged particle around a weakly magnetized naked singularity. *Int. J. Mod. Phys. D* **2016**, *25*, 1650024. [[CrossRef](#)]
36. Bañados, M.; Silk, J.; West, S.M. Kerr Black Holes as Particle Accelerators to Arbitrarily High Energy. *Phys. Rev. Lett.* **2009**, *103*, 111102. [[CrossRef](#)] [[PubMed](#)]
37. Majeed, B.; Jamil, M. Dynamics and center of mass energy of colliding particles around black hole in $f(R)$ gravity. *Int. J. Mod. Phys. D* **2017**, *26*, 1741017. [[CrossRef](#)]
38. Zakria, A.; Jamil, M. Center of mass energy of the collision for two general geodesic particles around a Kerr-Newman-Taub-NUT black hole. *J. High Energy Phys.* **2015**, *2015*, 147. [[CrossRef](#)]
39. Brevik, I.; Jamil, M. Black holes in the turbulence phase of viscous rip cosmology. *Int. J. Geom. Methods Mod. Phys.* **2019**, *16*, 1950030. [[CrossRef](#)]
40. De Laurentis, M.; Younsi, Z.; Porth, O.; Mizuno, Y.; Rezzolla, L. Test-particle dynamics in general spherically symmetric black hole spacetimes. *Phys. Rev. D* **2018**, *97*, 104024. [[CrossRef](#)]
41. Pugliese, D.; Valiente Kroon, J.A. On the evolution equations for ideal magnetohydrodynamics in curved spacetime. *Gen. Relativ. Gravit.* **2012**, *44*, 2785–2810. [[CrossRef](#)]
42. Pugliese, D.; Valiente Kroon, J.A. On the locally rotationally symmetric Einstein-Maxwell perfect fluid. *Gen. Relativ. Gravit.* **2016**, *48*, 74. [[CrossRef](#)]
43. Pugliese, D.; Quevedo, H.; Rueda, H.J.A.; Ruffini, R. Charged boson stars. *Phys. Rev. D* **2013**, *88*, 024053. [[CrossRef](#)]
44. Belvedere, R.; Pugliese, D.; Rueda, J.A.; Ruffini, R.; Xue, S.S. Neutron star equilibrium configurations within a fully relativistic theory with strong, weak, electromagnetic, and gravitational interactions. *Nucl. Phys. A* **2012**, *883*, 1–24. [[CrossRef](#)]
45. Stuchlík, Z.; Kološ, M.; Kovář, J.; Slaný, P.; Tursunov, A. Influence of Cosmic Repulsion and Magnetic Fields on Accretion Disks Rotating around Kerr Black Holes. *Universe* **2020**, *6*, 26. [[CrossRef](#)]
46. Misner, C.W.; Thorne, K.S.; Wheeler, J.A. *Gravitation*; W. H. Freeman: San Francisco, CA, USA, 1973.
47. Wald, R.M. Black hole in a uniform magnetic field. *Phys. Rev. D* **1974**, *10*, 1680–1685. [[CrossRef](#)]
48. Aliev, A.N.; Galtsov, D.V.; Petukhov, V.I. Negative absorption near a magnetized black hole - Black hole masers. *Astrophys. Space Sci.* **1986**, *124*, 137–157. [[CrossRef](#)]
49. Aliev, A.N.; Gal'tsov, D.V. Reviews of topical problems: “Magnetized” black holes. *Sov. Phys. Uspekhi* **1989**, *32*, 75–92. [[CrossRef](#)]
50. Aliev, A.N.; Özdemir, N. Motion of charged particles around a rotating black hole in a magnetic field. *Mon. Not. R. Astron. Soc.* **2002**, *336*, 241–248. [[CrossRef](#)]
51. Bicak, J.; Suchlik, Z.; Balek, V. The motion of charged particles in the field of rotating charged black holes and naked singularities. *Bull. Astron. Institutes Czechoslov.* **1989**, *40*, 65–92.
52. Novikov, I.D.; Thorne, K.S. Astrophysics of black holes. In *Black Holes (Les Astres Occlus)*; Dewitt, C., Dewitt, B.S., Eds.; CRC Press: Boca Raton, FL, USA, 1973; pp. 343–450.
53. Shakura, N.I.; Sunyaev, R.A. Black holes in binary systems. Observational appearance. *Astron. Astrophys.* **1973**, *24*, 337–355.
54. Pringle, J.E. Accretion discs in astrophysics. *Annu. Rev. Astron. Astrophys.* **1981**, *19*, 137–162. [[CrossRef](#)]
55. Bian, W.H.; Zhao, Y.H. Accretion Rates and the Accretion Efficiency in AGNs. *Publ. Astron. Soc. Jpn.* **2003**, *55*, 599–603. [[CrossRef](#)]
56. Miller, J.M.; Raymond, J.; Fabian, A.; Steeghs, D.; Homan, J.; Reynolds, C.; van der Klis, M.; Wijnands, R. The magnetic nature of disk accretion onto black holes. *Nature* **2006**, *441*, 953–955. [[CrossRef](#)]
57. Khan, S.U.; Chen, Z.M. Charged particle dynamics in black hole split monopole magnetosphere. *Eur. Phys. J. C* **2023**, *83*, 704. [[CrossRef](#)]
58. Zaslavskii, O.B. General properties of the Penrose process with neutral particles in the equatorial plane. *Phys. Rev. D* **2023**, *108*, 084022. [[CrossRef](#)]
59. Landau, L.D. *The Classical Theory of Fields*; Elsevier: Amsterdam, The Netherlands, 2013; Volume 2.
60. Reynolds, C.S.; Fabian, A.C. Broad Iron- $K\alpha$ Emission Lines as a Diagnostic of Black Hole Spin. *Astrophys. J.* **2008**, *675*, 1048–1056. [[CrossRef](#)]

61. Wilkins, D.R.; Reynolds, C.S.; Fabian, A.C. Venturing beyond the ISCO: Detecting X-ray emission from the plunging regions around black holes. *Mon. Not. R. Astron. Soc.* **2020**, *493*, 5532–5550. [[CrossRef](#)]
62. Reynolds, C.S. Observing black holes spin. *Nat. Astron.* **2019**, *3*, 41–47. [[CrossRef](#)]
63. Turimov, B.; Boboqambarova, M.; Ahmedov, B.; Stuchlík, Z. Distinguishable feature of electric and magnetic charged black hole. *Eur. Phys. J. Plus* **2022**, *137*, 222. [[CrossRef](#)]

Disclaimer/Publisher's Note: The statements, opinions and data contained in all publications are solely those of the individual author(s) and contributor(s) and not of MDPI and/or the editor(s). MDPI and/or the editor(s) disclaim responsibility for any injury to people or property resulting from any ideas, methods, instructions or products referred to in the content.